Clays and Clay Minerals, Vol. 43, No. 1, 29–38, 1995.

EVOLUTION OF HEMATITE SURFACE MICROTOPOGRAPHY UPON DISSOLUTION BY SIMPLE ORGANIC ACIDS

PATRICIA A. MAURICE,[1] MICHAEL F. HOCHELLA JR.,[1] GEORGE A. PARKS,[1]
GARRISON SPOSITO,[2] AND UDO SCHWERTMANN[3]

[1] Department of Geological and Environmental Sciences
Stanford University, Stanford, California 94305

[2] Department of Environmental Science, Policy, and Management
University of California at Berkeley, Berkeley, California 94720

[3] Institute of Soil Science, Technical University of Munich, Germany

Abstract—The surface microtopography of hematite over the course of dissolution in oxalic and citric acids was examined by *in-situ* and *ex-situ* atomic-force microscopy. *In-situ* imaging of the basal-plane surface of a centimeter-scale natural hematite sample immersed in 2 mM citric acid demonstrated that the basal-plane surface was relatively unreactive; rather, dissolution occurred along step edges and via etch-pit formation. *Ex-situ* imaging of synthetic hematite particles following batch dissolution in 1 mM oxalic acid showed similar dissolution features on basal-plane surfaces; in addition, etching along particle edges was apparent. The presence of etch features is consistent with a surface-controlled dissolution reaction. The results are in agreement with previous investigations suggesting that the basal-plane surface is relatively unreactive with respect to ligand exchange. Both *in-situ* and *ex-situ* imaging of particle surfaces can provide valuable information on the roles of surface structures and microtopographic features in mineral dissolution.

Key Words—Atomic force microscope, Clay mineral surfaces, Dissolution, Hematite, Organic acids.

INTRODUCTION

This paper focuses on the roles of mineral-surface structure and microtopography in the dissolution of hematite (α-Fe_2O_3) by oxalic and citric acids as an important step toward developing mechanistic models of iron-oxide dissolution by simple organic acids. Hematite is ubiquitous in soils and sediments and often forms coatings on mineral grains (Berner and Schott 1982, Rude and Aller 1989). Its surface structure, composition, and reactivity have been studied by a variety of surface-analytical techniques (Parks and De Bruyn 1962, Parfitt *et al* 1975, Barron *et al* 1988, Lad and Henrich 1989, Johnsson *et al* 1991, Eggleston and Hochella 1992). Oxalic and citric acids are two of the most important simple organic acids found in forested soils (Fox and Comerford 1990). Their sorption to hematite (Kallay and Matijević 1985, Zhang *et al* 1985) and their effects on the dissolution (Waite and Morel 1984, Zhang *et al* 1985, Miller *et al* 1986, Cornell and Schindler 1987, Suter *et al* 1988) and growth (Schwertmann *et al* 1968, Fisher and Schwertmann 1975) of hematite and other hydrous iron oxides have been studied extensively.

The rates of iron-oxide dissolution by simple organic acids appear to be surface controlled (Zhang *et al* 1985, Stumm *et al* 1985, Sulzberger *et al* 1989). Iron-oxide dissolution rates increase with increasing organic-ligand adsorption and decreasing pH (Zhang *et al* 1985). Ligand adsorption itself increases, as expected (Parks 1990), with increasing ligand concentration and decreasing pH (Zhang *et al* 1985). Dissolution rates also increase with increasing temperature, implying a reaction with substantial activation energy (Zhang *et al* 1985). Observations of etch pits on hematite particles derived from anaerobic soils (Bigham *et al* 1990) are consistent with a surface-controlled dissolution mechanism (Berner 1980), although the role of organic ligands in the etch-pit formation is not known. More than one reaction may contribute to the overall dissolution rate (Sulzberger *et al* 1989).

Stumm and Wieland (1990) proposed that non-reductive dissolution of iron oxides by simple hydroxycarboxylic acids proceeds through the formation of a metal-organic chelate surface complex, which is a precursor to an activated surface complex. If the dissolution of hematite by simple organic acids is indeed surface-controlled, with dissolution proceeding through the formation of an Fe-organic surface chelate (Stumm 1992), then dissolution rates should be influenced not only by the nature and concentration of the ligand and by solution conditions, but also by the structure, composition, and chemical reactivity of the mineral surface (Eggleston *et al* 1989, Hochella 1990). By analogy with inorganic systems (Berner and Holdren 1977, Casey *et al* 1988), dissolution should occur preferentially at high-energy sites on the hematite surface (Stumm and Wieland 1990). Such high-energy sites or "active sites" on the surface may include dislocations, microfractures, edges, point defects, kinks, and grain or twin boundaries (Helgeson *et al* 1984). In addition to the ease of

removing Fe atoms from high-energy sites, steps, kinks, and edges may be more favorable locations for the adsorption of organic molecules which is the first step in the dissolution process. Steps and kinks offer two and three edges to solution, respectively, rather than just one as along a flat surface. Hence, the adsorption of organic molecules at steps and kinks may result in a smaller increase or a larger decrease in surface free energy (Blum and Lasaga 1987). In addition, because the coordination chemistry of hematite varies with crystallographic face (Barron *et al* 1988), experimentally determined dissolution rates may vary for particles with different aspect ratios. Thus, evaluating the influence of surface heterogeneity on dissolution processes is a crucial step toward interpreting dissolution-rate data (Brantley *et al* 1986, Wehrli 1989), identifying reaction mechanisms (Helgeson *et al* 1984), and comparing rates and mechanisms of reactions in the laboratory and the field (Brantley *et al* 1986, Blum and Lasaga 1991).

Although the potential importance of different surface sites in hematite dissolution by simple organic acids has been recognized (Stumm and Wieland 1990), our ability to evaluate the importance of surface heterogeneity has been limited by the lack of high-resolution techniques for imaging mineral surfaces *in situ* over the course of dissolution. Atomic-force microscopy (AFM) has emerged as a technique for direct, nanometer-scale imaging of mineral surfaces immersed in aqueous solution (Binnig *et al* 1986, Johnsson *et al* 1991, Hillner *et al* 1992a, 1992b, Gratz *et al* 1993, Dove and Hochella 1993, Ohnesorge and Binnig 1993) and of particulate mineral surfaces in air (Hartman *et al* 1990, Lindgreen *et al* 1991, Blum and Eberl 1992). In this paper, we describe experiments wherein AFM was utilized to: (1) image *in situ* the basal-plane surface microtopography of single-crystal hematite over the course of reaction with a citric-acid solution; and (2) image *ex situ* at nanometer-scale resolution the surfaces of hematite particles following their reaction with oxalic-acid solutions for time periods ranging from 2 to >60 hours.

EXPERIMENTAL

Sample materials

A Brazilian specular hematite (α-Fe_2O_3) specimen from the Stanford Mineral Collection was used in the *in-situ* experiment. The hematite displayed well developed {001} parting and could be fractured to produce mirror-flat surfaces prior to imaging. No other sample preparation was necessary.

Synthetic hematite particles for the *ex-situ* experiments were synthesized from an $Fe(NO_3)_3$ solution (Schwertmann and Cornell 1991). B.E.T. measurements performed with a Micrometrics Flowsorb II 2300 N_2 analyzer gave a surface area of 40 m^2/g. X-ray diffractograms showed good agreement with standard hematite diffraction patterns. Surface-chemical analysis by X-ray photoelectron spectroscopy (XPS) performed with a VG ESCALAB Mark II using Al Kα radiation showed no evidence of contamination by NO_3, Al, Si, Mn, or other common impurities (Maurice-Johnsson 1993).

Atomic-force microscopy

A Nanoscope II Model AFM-1 atomic-force microscope manufactured by Digital Instruments was used in these experiments. Design and operation of the AFM in air and static aqueous solutions has been described in detail elsewhere (Hochella *et al* 1990, Johnsson *et al* 1991); operation in a flow-through system is described below.

In-situ dissolution experiment

For the *in-situ* experiment, a gravity flow-through system was used (Figure 1). The sample was imaged for several minutes in deionized water, after which the fluid cell was flushed momentarily with 0.002 M citric acid. A slow flow rate (~1 ml/hour) of 0.002 M citric acid was maintained for the remainder of the experiment. The slow flow rate was chosen to minimize flow-related disturbance of the tip/sample interactions including increased drift. The initial solution was 0.002 M citric acid, and had a pH upon equilibration with air of ~3.1. The citric-acid solution was open to the atmosphere, and was not buffered. The effluent solution was exposed in outflow lines to potential mixing with deionized water; well flushed portions were too small to permit chemical analysis following reaction. Twice during the experiment, the tip was disengaged from the surface for three minutes to assess whether the observed dissolution features were scan-related (e.g., whether the tip was eroding the sample surface). The experiment was conducted in the dark, except for the laser light (670 nm), in order to prevent photocatalyzed reductive dissolution.

Batch (ex-situ) dissolution experiments

The dissolution experiments of particulate hematite in 0.001 M oxalic acid at pH 3 and 4 and ionic strength 0.008 M are described by Maurice-Johnsson (1993). Briefly, the experiments were conducted in a batch reaction vessel consisting of a 100 ml Teflon® beaker immersed in a double-jacketed vessel. Solution volumes = 50 ml; weight of solid = 0.10 g. Solution pH was maintained at pH 3 or 4 for the first two hours of reaction using a computer-controlled pH-stat system, after which the electrodes (glass and reference) were removed in order to prevent substantial contamination by electrode fill solution. Most proton consumption occurred in the first two hours, and subsequent pH drift was <0.1 pH unit. Temperature was maintained at 22.0° ± 0.4°C. In order to limit reductive dissolution,

https://doi.org/10.1346/CCMN.1995.0430104 Published online by Cambridge University Press

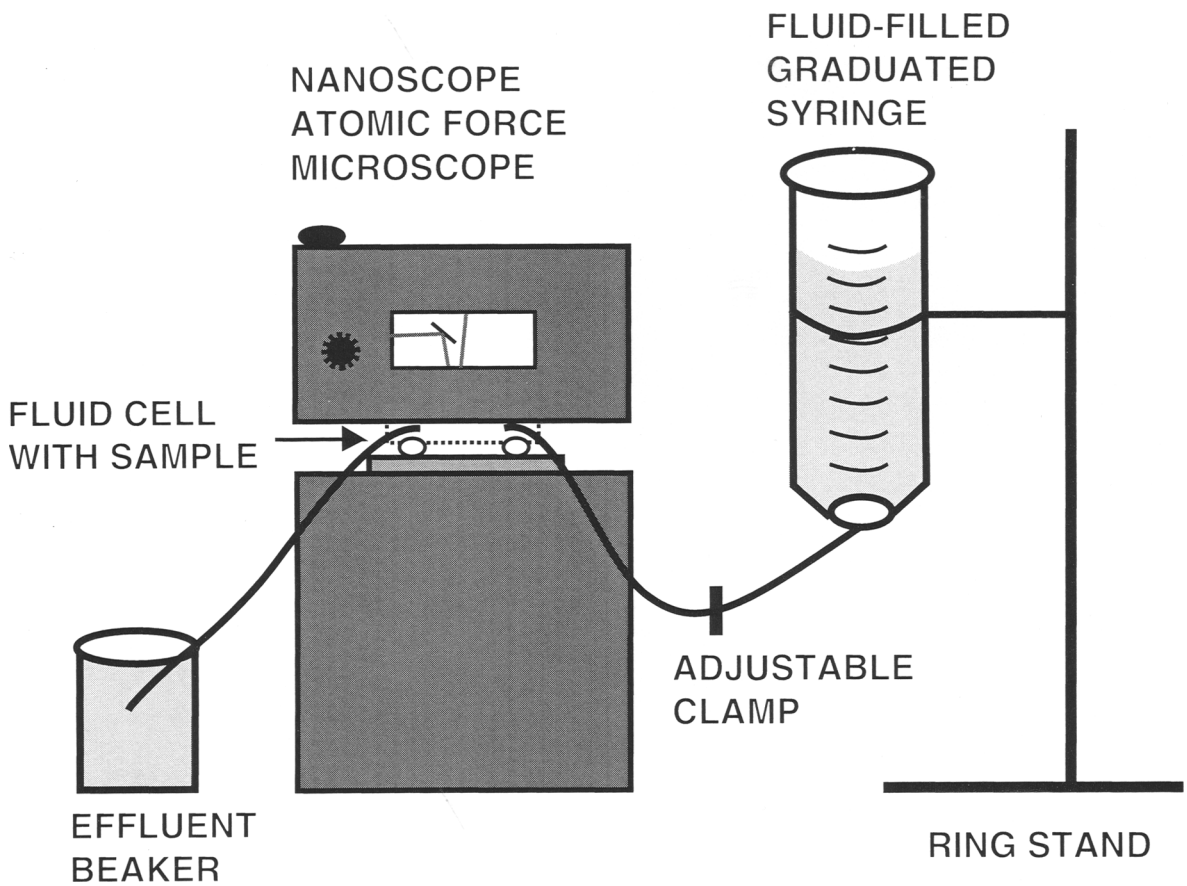

Figure 1. Gravity flow-through system used in the *in-situ* dissolution experiment. A graduated syringe containing 0.002 M citric acid, pH = 3.1 was attached to a line leading to the fluid cell of the Digital Instruments Model AFM-1. A small clamp attached to the input line was used to regulate the flow.

all experiments were conducted in the dark and exposed to the atmosphere. Separate experiments were conducted for each time period.

Following reaction for a given time period, particle suspensions were filtered through a syringe filter containing 0.1 or 0.2-μm pore-diameter Nucleopore® polycarbonate membrane filters. The filter papers were rinsed with 1 ml deionized water and then allowed to air-dry under cover. AFM imaging required dispersed particles. In cases where particle density on the filter surface was too great, the excess particles were lightly brushed off the surface. Following filtration, sample solutions were analyzed for Fe with a Perkin-Elmer model 403 atomic absorption spectrophotometer (AA) equipped with a graphite furnace.

RESULTS

In-situ experiment

Results of the *in-situ* dissolution experiment of specular hematite immersed in 0.002 M citric acid are shown in Figure 2. Figure 2a shows the surface at the beginning of the experiment, in deionized water. The surface consists of a set of parallel steps, with the step edges running diagonally from the upper left to the lower right. The average step interval parallel to the parting surface is 1500 nm. Step heights are distorted (increased) because the basal-plane surfaces are inclined slightly relative to the tip. Hysteresis in the instrumental feedback loop which keeps the height of the sample under the tip approximately constant also contributes to the distortion. However, repeated measurements after low-pass filtering and planefitting of the data permitted estimation of the average step height as 15 $\pm$ 10 nm. Given that the unit cell dimension c_o for hematite is 1.373 nm, the steps average more than 10 unit cells in height. The surface also contains several "islands". The thick, rough-edged steps and islands are typical of growth structures found on the basal-plane surfaces of many natural specular hematite samples (Sunagawa 1962).

Figures 2b–d show the surface following brief flushing of the fluid cell with 0.002 M citric acid and under conditions of slow flow. The scan direction was changed

https://doi.org/10.1346/CCMN.1995.0430104 Published online by Cambridge University Press

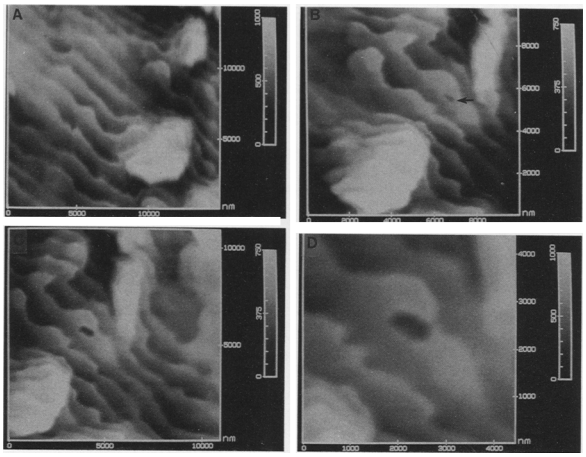

Figure 2. Results of the *in-situ* dissolution experiment on the basal-plane surface of single-crystal specular hematite. All scales in nanometers (nm). (a) Sample surface in deionized H_2O. The surface contains a series of rough-edged steps with an average step interval of ~1500 nm and an average step height of ~15 ± 10 nm. Terraces to the left of the step edges are topographically higher than terraces to the right. Several small islands, one of which contains spiral steps, also are apparent. (b) Sample surface (image shifted; the large island provides reference) approximately 15 minutes after H_2O was replaced by 0.002 m citric acid. A small pit (see arrow) has begun to form along one terrace. In (c), taken 34 minutes after introduction of citric acid, the pit has grown and taken on a roughly hexagonal outline. Pit depth is ~200 nm. Step edges have receded slightly (see Figure 3). (d) Is a close-up of the pit, 8 minutes later.

Figure 3. Tracing of features in Figure 2b and 2c, showing pit growth and retreat of steps. What appears to be a slight step growth near the edges of the figure probably is due to image drift rather than actual growth.

by 90°, and the scan size decreased from 15,000 nm to 10,000 nm in going from (a) to (b), resulting in a shift of the image area and a slight change in the shapes of features caused by a change in directional drift components and heterogeneous tip shape. The large island in the lower right of Figure 2a (photograph was rotated 90° to facilitate comparison) is shifted toward the left of Figure 2b. Several changes in surface microtopography occurred as dissolution proceeded. Figure 3 illustrates the changes in the edges of features over 19 minutes (Figure 2b–c). At one point during this interval, the tip was lifted from the sample surface for about three minutes, and, upon re-engagement, the image area was shifted slightly. Comparison of surface features along the edges in Figure 3 is not as reliable as near the center because of slightly increased drift effects near the edges.

The most striking change in surface microtopography was a small pit that nucleated and grew on one terrace (see arrow in Figure 2b). The initial pit shape was elongated roughly parallel to the overall trend of the step edges. As the pit continued to grow, it took on an approximately hexagonal outline (Figure 2d), consistent with the hexagonal symmetry of hematite. The pit appeared to be flat-bottomed, and the pit walls appeared to be steep and not terraced.

The shape and depth (~200 nm) of the pit are consistent with nucleation at a dislocation. If the pit nucleated at an impurity, pit depth probably would have been on the order of Ångstroms, not hundreds of nanometers (Blum and Lasaga 1987, Johnsson *et al* 1992). Given that the pit is flat-bottomed, there must have been a discontinuity in the crystal structure parallel to the basal-plane surface, such that the dislocation was terminated at depth. Such a discontinuity is reasonable considering the well-developed parting parallel to the basal-plane surface. It is not surprising that we were able to image one dislocation-associated pit in the image area. The dislocation density calculated from the image area would be 6×10^4 cm^{-2}, a reasonable dislocation density for natural mineral samples (Blum *et al* 1990). Because this calculated density is based on only one image area, it should not be taken as a representative dislocation density.

Theories of dislocation-related etch pit nucleation and growth have been reviewed recently (Lasaga and Blum 1986, Brantley *et al* 1986, Blum *et al* 1990, MacInnis and Brantley 1992). In brief, and using the notation of MacInnis and Brantley (1992), the for-

https://doi.org/10.1346/CCMN.1995.0430104 Published online by Cambridge University Press

mation of an etch pit is favored by the Gibbs energy gain associated with dissolution of a given volume of the crystal structure (ΔG_{vol}), but this favorable Gibbs energy gain is countered by an increase in surface Gibbs energy (ΔG_{surf}) as new surface area is formed along the walls. Hence,

$$\Delta G_{perf} = -\Delta G_{vol} + \Delta G_{surf} \quad (4)$$

where ΔG_{perf} refers to the free energy associated with dissolution at a perfect area of the crystal, free of high-energy sites such as steps, kinks, impurities, and dislocations. A negative sign is given to ΔG_{vol} because for the solution conditions in which dissolution is favored, it will decrease the total Gibbs energy.

As the diameter of the pit increases, the incremental increase in surface area decreases such that ΔG_{surf} tends toward a smaller and smaller value. Dissolution can occur most readily at high-energy sites on crystal surfaces; in the case of dislocations, the elastic strain energy (ΔG_{str}) associated with the dislocation is available to decrease the free energy associated with nucleation of a pit. Hence, the Gibbs energy equation for a portion of the surface containing a dislocation (dis) will contain an extra term:

$$\Delta G_{dis} = -\Delta G_{vol} + \Delta G_{surf} - \Delta G_{str} \quad (5)$$

This strain energy is greatest at the core of the dislocation, but decreases greatly by about 10 Å from the dislocation line (Blum *et al* 1990). Thus, when a pit nucleates in the immediate region of a dislocation, the favorable energies associated with dissolution of a given volume of material ($-\Delta G_{vol}$) and with decrease in strain energy ($-\Delta G_{str}$) as the dislocation core is dissolved are countered by the unfavorable Gibbs energy associated with formation of additional surface area ($+\Delta G_{surf}$). As the pit expands, both the favorable release in strain energy and the unfavorable increase in surface free energy fall off rapidly. As pointed out by Blum *et al* (1990), as the pit continues to grow beyond a critical radius, the edges of the pit can be thought of as steps, which may be favorable sites for additional dissolution.

The changes in shape of the pit thus can be rationalized in terms of nucleation along a dislocation. Initial rapid nucleation along the line of the dislocation could account for the initial elongated shape of the pit; once pit edges form, they can be sites of crystallographically controlled dissolution leading to an expansion of the pit into a roughly hexagonal outline. The large depth of the pit can be accounted for by an extensive dislocation. Further analysis is needed to account for the steep-edged walls of the pit; for example, results of Monte Carlo simulations (e.g., Blum and Lasaga 1987) could be compared with AFM images.

Dissolution also occurred along step edges. Over 19 minutes (Figure 3), the step edges retreated an average of 30 nm; average step retreat velocity was 0.026 nm

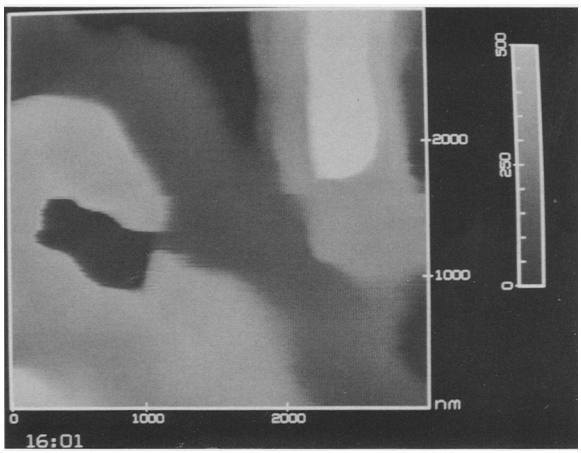

Figure 4. Image of the pit shown in Figure 3d, following several minutes of small-scan imaging. Scan-induced erosion of the pit resulted in alignment of pit edges with scan direction and distortion of the original hexagonal shape.

s^{-1}. Step-edge retreat was not uniform but varied from <5 nm to >100 nm from place to place along the step edges. The steps appeared to recede as a whole, without splitting into multiple smaller steps. Our observation of step retreat is in agreement with an *ex-situ* phase contrast microscopy study by Sunagawa (1987), in which lateral migration of steps across the basal-plane surface was observed as dissolution proceeded. An estimate of the contribution from dissolution along steps to the dissolution rate is 0.02 mg Fe $m^{-2}h^{-1}$. This dissolution rate does not include the contribution from the etch pit. If a depth of 200 nm is taken for the etch pit, then an additional contribution of 0.08 mg Fe $m^{-2}h^{-1}$ is added to give a total dissolution rate of 0.10 mg Fe $m^{-2}h^{-1}$. For comparison, we calculate from Zhang *et al*'s (1985) batch dissolution data the mean dissolution rate of synthetic particulate hematite in 0.02 M citric acid at pH 3 over a reaction period of 17 hours. Their mean dissolution rate is 0.001 mg Fe $m^{-2}h^{-1}$. Our mean dissolution rate is two orders of magnitude greater, despite a one order of magnitude smaller citric-acid concentration. A fast rate is expected in our experiment because it is an initial dissolution rate on a freshly cleaved surface with a high density of reactive surface sites.

Near the end of the experiment, the scan area was decreased to the region immediately surrounding the pit. During this procedure, the pit edges began to align with the scan direction (Figure 4), suggesting that scan-induced erosion occurred during the small-region scans. Erosion during small-region scans can be a problem because of the rapid scan rate needed to compensate for drift at high resolution (Barrett 1991). Because dissolution continued when the tip was temporarily lifted (withdrawn) from the sample surface, we believe that the microtopographic changes observed during large

https://doi.org/10.1346/CCMN.1995.0430104 Published online by Cambridge University Press

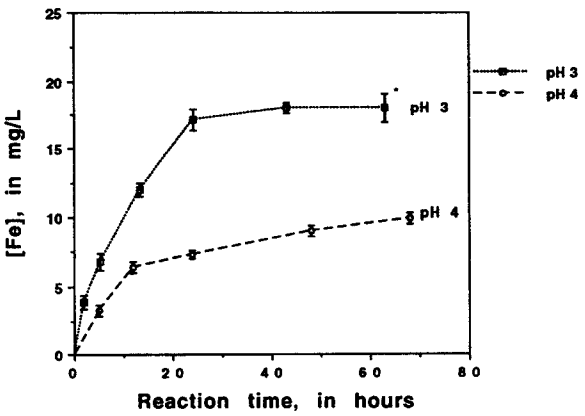

Figure 5. Results of batch dissolution experiments at pH = 3 and 4, I ~ 0.008 M, T = 22 ± 0.2°C, showing Fe concentration in solution at different reaction times.

area scans (as outlined in Figure 3) were caused primarily by dissolution. We recommend the following procedures for *in-situ* imaging: (1) use as low a force and as slow a scan speed as possible; (2) occasionally withdraw the tip from the sample surface, or image one small region for a brief interval to give the larger region a rest from scanning; (3) periodically change scan direction and look for alignment of features with scan, and (4) carefully examine images for alignment of features with scan direction and for changes in apparent reaction rates as a function of imaging parameters (e.g., force; scan size, speed, and direction).

Ex-situ experiments

Results of the dissolution experiments are shown in Figure 5. The initial dissolution rate was high but the rate of Fe accumulation in solution decreased over time. The hematite particles used in these experiments were synthetic, not ground from a natural specimen. Hence, the effects of ultrafine particles and grinding-induced high-energy sites (e.g., Petrovich 1981) on the initial dissolution rate should have been minimized. The high initial dissolution rate may be related to an abundance of free oxalate in the initial solution or to the initial solution being the most undersaturated; the latter plateau in [Fe] could be related to the decrease in free and sorbed oxalate concentrations as oxalate became bound to Fe in solution, and/or to back reactions, including secondary-phase formation. Sorption measurements showed that from 5 to 24 hours reaction time at pH 3, the amount of sorbed oxalate decreased by approximately 60% (see Maurice-Johnsson 1993).

In batch dissolution experiments, steady-state rates cannot be calculated (Holdren and Speyer 1985, Chou and Wollast 1984, Rimstidt and Dove 1986) because a variety of processes besides dissolution (e.g., back reaction, sorption, and secondary phase formation) may contribute to the curve of dissolved iron concentration *versus* time. Although this is a disadvantage of batch experiments, the potential accumulation of reaction products is consistent with soil processes. Secondary phase formation may have contributed to the surface microtopography observed by AFM. Nevertheless, in agreement with previous studies of hydrous iron oxide dissolution in oxalic acid, we observed substantial dissolution, with the amount of iron released to solution at any given time greater at pH 3 than at pH 4.

Imaging particulate materials by AFM is difficult because the tip shape can convolute with the shapes of particle edges, particles can be swept away by the tip, and particles can adhere to or damage the end of the tip, destroying image quality. Although we were able to obtain numerous images of particles, we were unable to obtain enough high quality, clear images of complete grains (e.g., with no edges obscured and nanometer-scale resolution), to allow quantitative comparison with solution data. Prior to reaction with oxalic acid (Figure 6a), particle shapes typically were hexagonal and rhombohedral, with particle diameters ranging from 100 nm to 2000 nm. Some straight-edged steps were apparent on the basal-plane surfaces. No etch pits were observed on the basal-plane surfaces or along particle edges. Following reaction, two different types of apparent dissolution feature were observed on the basal-plane surfaces: (1) small etch pits with either rounded or unresolved shapes (Figure 6d, e, f, i, j); and (2) shallow, ~1-unit-cell high steps with irregular edges that intersect particle edges (Figure 6b and 6c) and might have formed by migration of a unit-cell-high step from the edge of the grain across the particle surface. In addition, at reaction times > 24 hours, we observed some etching along particle edges (non-basal-plane surfaces) (Figure 6g–i), and particle surfaces often were rough-looking and increasingly difficult to image. The pits observed on the basal-plane surface were difficult to image at high resolution; uncertainties regarding shape and depth make it difficult to determine whether the pits nucleated at dislocations or at point defects or impurities. Some large, straight-edged steps were present on the initial (unreacted) surfaces. Whether or not these large steps retreated during dissolution could not be discerned from the *ex-situ* imaging because there was no reference against which to measure motion.

DISCUSSION

The *in-situ* dissolution experiment demonstrated that the bulk of the basal-plane surface of hematite is unreactive with respect to dissolution in citric and oxalic acids. Dissolution occurred primarily by the retreat of step edges across the basal-plane surface and the formation of etch pits. The *ex-situ* experiments showed

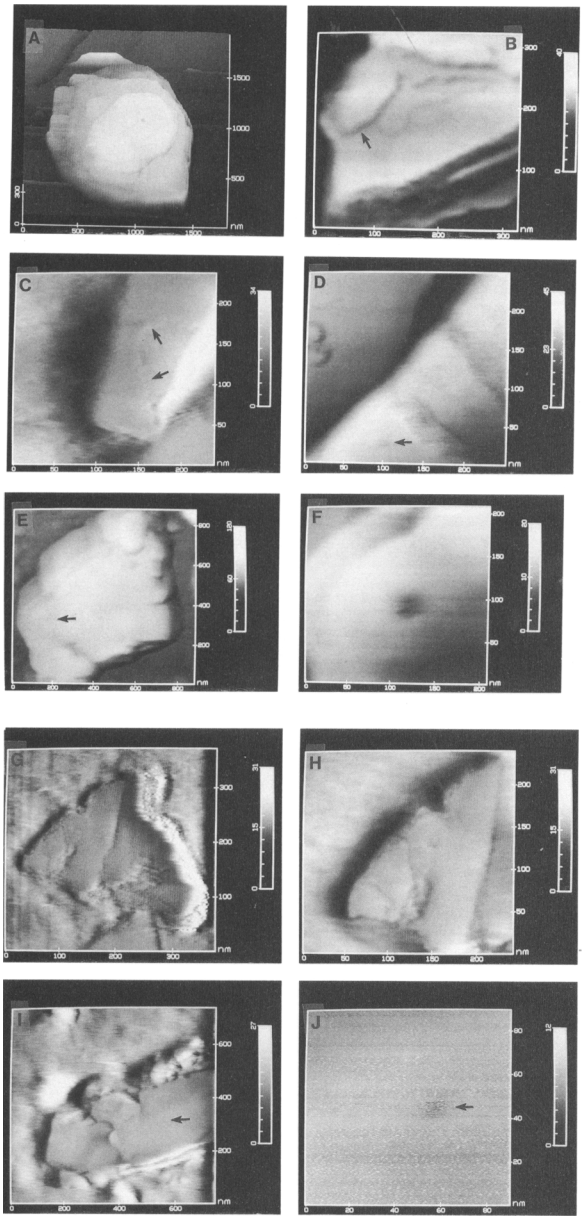

Figure 6. AFM images in air of hematite particles deposited on polycarbonate membrane filter. (a) An unreacted hematite particle. The left edge of the particle contains striations which are an artifact, most probably caused by the tip sticking slightly to the edge of the particle. (b) A shallow (~1 unit-cell-high) etched-out region on the basal-plane surface of a particle reacted with 0.001 M oxalic acid at pH 4 for 26 hours (arrow is on topographically lower side of step); (c) Another shallow (~1-unit-cell high) etched out region along the edge of a hematite particle reacted in 0.001 M oxalic acid at pH 3 for 43 hours (arrows are on topographically lower side of step). The light region along the right edge of the particle is an artifact of the tip edge riding over a steep surface feature. (d) A small rounded pit along a terrace on a particle reacted with 0.001 M oxalic acid at pH 4 for 26 hours. (e) Small, rounded pits on the basal-plane surface of a hematite particle reacted with 0.001 M oxalic acid at pH 4 for 6.5 h; (f) is a close-up along the upper left edge of (e). The upper left edge of the particle

etch pits and rough-edged steps on the basal-plane surface, consistent with the results of the *in-situ* experiments. However, the *ex-situ* experiments permitted imaging of particle edges, revealing pits and a generally roughened outline of particle edges (prismatic faces). Step edges and pit walls expose non-basal-plane (prismatic) surfaces to solution; hence, dissolution along step edges, pit walls, and particle edges all point to increased reactivity of the prismatic surfaces relative to the basal-plane surface.

These observations are in agreement with the known effects of citrate on hematite crystal growth. Schwertmann *et al* (1968) demonstrated that citrate alters the shapes of hematite particles grown from solution. In the absence of citrate, particles display platey habits with the basal-plane surface predominant, whereas in the presence of citrate, particles display needle-like habits, with the prismatic-plane surfaces predominant. Schwertmann *et al* (1968) attributed these differences to preferential citrate adsorption on the prismatic planes. Studies of phosphate sorption also have shown that the basal-plane surface of hematite is relatively unreactive compared with the prismatic surfaces. Phosphate is believed to sorb to hematite by a ligand-exchange mechanism involving hydroxyl groups on the hematite surface (Goldberg and Sposito 1985). Barron *et al* (1988) showed that the amount of phosphate sorption correlated positively with the aspect ratios of hematite particles: sorption increased as the proportion of non-basal-plane surfaces to basal-plane surfaces increased. They attributed the increased sorption to the presence of monocoordinated hydroxyls on the non-basal (110), (100), and (223) surfaces and to the absence of monocoordinated hydroxyls on the basal (001) surfaces. Citric and oxalic acids also are believed to sorb by ligand-exchange mechanisms (e.g., Kallay and Matijević 1985, Stumm 1992), although differing affinity for the basal- *versus* non-basal surfaces has not yet been demonstrated. The results of our experiments are consistent with a different reactivity of the basal *versus* non-basal-plane surfaces with respect to dissolution in citric and oxalic acids, perhaps resulting from different sorption densities or mechanisms. Correlations between sorption densities of simple organic acids and dissolution rates of hydrous iron oxides (e.g., Stumm

←

may show convolution of the tip shape with the particle shape, and may not be representative of true structure. (g) A particle reacted in 0.001 M oxalic acid at pH 3 for 43 hours. The surface is rough and was difficult to image, perhaps due to dissolution and/or secondary-phase formation. Pitting along particle edges is apparent in this image and in the close-up shown in (h). (i) Another particle reacted in 0.001 M oxalic acid at pH 3 for 43 hours. A small pit just to the right of center is shown at high resolution in (j). As shown in (j), small-scan images on these particle surfaces often lacked clarity.

https://doi.org/10.1346/CCMN.1995.0430104 Published online by Cambridge University Press

and Wieland 1990) suggest that sorption is an important step in the dissolution process.

CONCLUSIONS

In-situ and *ex-situ* AFM images of changes in hematite microtopography upon reaction with dilute solutions of citrate and oxalate demonstrate that:

(1) There is evidence for dissolution at specific microtopographic features and "high energy" sites, consistent with a surface-controlled dissolution mechanism.
(2) Dissolution occurs simultaneously at more than one type of feature (pit and step) on the basal-plane surface, as well as along particle edges. Hence, reactions at more than one type of microtopographic site may contribute to the overall observed dissolution rate. The role of atomic-scale coordination remains a subject of ongoing research.
(3) The basal-plane surface appears to be relatively unreactive under experimental conditions. Dissolution along pit walls, step edges, and particle edges suggests that prismatic surfaces are more reactive than are basal-plane surfaces.
(4) *In-situ* and *ex-situ* experiments show consistent dissolution features (step retreat and pit growth), suggesting that the observations are real and not instrumental artifacts.

The results of this study demonstrate that *in-situ* and *ex-situ* AFM imaging of particle surfaces during and after dissolution provides valuable information on the roles of surface structures and microtopographic features in mineral dissolution. The *in-situ* imaging was particularly important in identifying retreat of step-edges as an important process that otherwise might have been overlooked because dissolution steps may be difficult to distinguish from growth steps. Although nanometer-scale imaging of particulate materials can be difficult, recent advances in AFM techniques, including operation with an optical microscope attachment, and development of sharper tips and development of tapping-mode atomic force microscopy (Zhong *et al* 1993) which reduces frictional forces between the tip and the sample all promise to make such imaging easier, and to allow quantitative analysis. Although imaging of single-crystal surfaces allows for direct observation of changes in surface microtopography over the course of reaction, imaging of particulate materials is important because for relatively unreactive materials such as hematite, particulate materials are needed to provide enough surface area for macroscopic rate determinations. With ongoing advances in AFM technology, quantitative comparison of dissolution rate and volume of dissolution features should eventually be possible.

ACKNOWLEDGMENTS

We thank the McGee Fund of Stanford University, the National Science Foundation Graduate Fellowship program, and the Petroleum Research Fund of the American Chemical Society for funding this research. Gratitude is expressed to G. Redden (Stanford University) for designing and helping to construct the pH-stat system. Discussions with A. Blum (U.S. Geological Survey), C. Eggleston (EAWAG, Switzerland), W. Stumm (EAWAG, Switzerland), P. Schindler (University of Bern, Switzerland), and W. Casey (U.C. Davis) contributed greatly to the design of the experiments and to the interpretation of the experimental results.

REFERENCES

Barrett, R. C. 1991. Development and applications of atomic force microscopy: Ph.D. dissertation. Stanford University.

Barron, V., M. Herruzo, and J. Torrent. 1988. Phosphate adsorption by aluminous hematites of different shapes. *Soil Sci. Soc. of Amer. J.* **52**: 647–651.

Berner, R. A., and G. R. Holdren. 1977. Mechanism of feldspar weathering: Some observational evidence. *Geology* **5**: 369–372.

Berner, R. A. 1980. *Early Diagenesis.* Princeton, NJ: Princeton University Press, 241 pp.

Berner, R. A., and J. Schott. 1982. Mechanism of pyroxene and amphibole weathering—II. Observations of soil grains. *Amer. J. of Sci.* **282**: 1214–1231.

Bigham, J. M., S. E. Heckendorn, N. E. Smeck, and W. F. Jaynes. 1990. Relative stability of iron oxides in two soils with contrasting colors. *Soil Sci. Soc. Amer. J.* **55**: 1485–1492.

Binnig, G., C. F. Quate, and C. Gerber. 1986. Atomic force microscope. *Phys. Rev. Lett.* **56**: 930–933.

Blum, A. E., and D. D. Eberl. 1992. Determination of clay particle thicknesses and morphology using scanning force microscopy. In *Water-Rock Interaction VII.* Y. F. Kharaka and A. S. Maest, eds. Rotterdam: Balkema, 133–140.

Blum, A. E., and A. C. Lasaga. 1987. Monte Carlo simulations of surface reaction rate laws. In *Aquatic Surface Chemistry.* W. Stumm, ed. New York: John Wiley and Sons, 255–292.

Blum, A. E., and A. C. Lasaga. 1991. The role of surface speciation in the dissolution of albite. *Geochim. Cosmochim. Acta* **55**: 2193–2201.

Blum, A. E., R. A. Yund, and A. C. Lasaga. 1990. The effect of dislocation density on the dissolution rate of quartz. *Geochim. Cosmochim. Acta* **54**: 283–298.

Brantley, S. L., S. R. Crane, D. A. Crerar, R. Hellmann, and R. Stallard. 1986. Dissolution at dislocation etch pits in quartz. *Geochim. Cosmochim. Acta* **50**: 2349–2361.

Casey, W. C., M. J. Carr, and R. A. Graham. 1988. Crystal defects and the dissolution kinetics of rutile. *Geochim. Cosmochim. Acta* **52**: 1545–1556.

Chou, L., and R. Wollast. 1984. Study of the weathering of albite at room temperature and pressure in a fluidized bed reactor. *Geochim. Cosmochim. Acta* **48**: 2205–2217.

Cornell, R. M., and P. W. Schindler. 1987. Photochemical dissolution of goethite in acid/oxalate solution. *Clays & Clay Miner.* **35**: 347–352.

Dove, P. M., and M. F. Hochella Jr. 1993. Calcite precipitation mechanisms and inhibition by orthophosphate: In situ observations by scanning force microscopy. *Geochim. Cosmochim. Acta* **57**: 705–714.

Eggleston, C. M., M. F. Hochella, and G. A. Parks. 1989. Sample preparation and aging effects on the dissolution rate and surface composition of diopside. *Geochim. Cosmochim. Acta* **54**: 797–803.

Eggleston, C. M., and M. F. Hochella Jr. 1992. The structure of the hematite {001} surfaces by scanning tunneling microscopy: Image interpretation, surface relaxation, and step structure. *Amer. Miner.* **77**: 911–922.

Fisher, W. R., and U. Schwertmann. 1975. The formation of hematite from amorphous iron(III) hydroxide. *Clays & Clay Miner.* **23**: 33–37.

Fox, T. R., and N. B. Comerford. 1990. Low-molecular-weight organic acids in selected forest soils of the southeastern USA. *Soil Sci. Soc. Amer. J.* **54**: 1139–1144.

Goldberg, S., and G. Sposito. 1985. On the mechanism of phosphate adsorption by hydroxylated mineral surfaces: A review. *Commun. Soil Science Plant Anal.* **16**: 801–821.

Gratz, A. J., P. E. Hillner, and P. K. Hansma. 1993. Step dynamics and spiral growth on calcite. *Geochim. Cosmochim. Acta* **57**: 491–495.

Hartman, H., G. Sposito, A. Yang, S. Manne, S. A. C. Gould, and P. K. Hansma. 1990. Molecular-scale imaging of clay mineral surfaces with the atomic force microscope. *Clays & Clay Miner.* **38**: 337–342.

Helgeson, H. C., W. M. Murphy, and P. Aagaard. 1984. Thermodynamic and kinetic constraints on reaction rates among minerals and aqueous solutions: I. Rate constants, effective surface area, and the hydrolysis of feldspar. *Geochim. Cosmochim. Acta* **48**: 2405–2432.

Hillner, P. E., A. J. Gratz, S. Manne, and P. K. Hansma. 1992a. Atomic-scale imaging of calcite growth and dissolution in real-time. *Geology* **20**: 359–362.

Hillner, P. E., S. Manne, A. J. Gratz, and P. K. Hansma. 1992b. AFM images of dissolution and growth on a calcite crystal. *Ultramicroscopy* **42-44**: 1387–1393.

Hochella, M. F. Jr. 1990. Atomic structure, microtopography, composition, and reactivity of mineral surfaces. In *Mineral-Water Interface Geochemistry*. M. F. Hochella Jr. and A. F. White, eds. Mineralogical Society of America, 87–132.

Hochella, M. F. Jr., C. M. Eggleston, V. B. Elings, and M. S. Thompson. 1990. Atomic structure and morphology of the albite (010) surface. An atomic-force microscope and electron diffraction study. *Amer. Miner.* **75**: 723–730.

Holdren, G. R., and P. M. Speyer. 1985. pH dependent change in the rates and stoichiometry of dissolution of an alkali feldspar at room temperature. *Amer. J. Sci.* **285**: 994–1026.

Johnsson, P. A., C. M. Eggleston, and M. F. Hochella Jr. 1991. Imaging molecular-scale structure and microtopography of hematite with the atomic force microscope. *Amer. Miner.* **76**: 1442–1445.

Johnsson, P. A., M. F. Hochella Jr., G. A. Parks, A. E. Blum, and G. Sposito. 1992. Direct observation of muscovite basal-plane dissolution and secondary phase formation: An XPS, LEED, and SFM study. In *Water-Rock Interaction VII*. Y. K. Kharaka and A. S. Maest, eds. Rotterdam: A. A. Balkema, 159–162.

Kallay, N., and E. Matijević. 1985. Adsorption at solid/solution interfaces. 1. Interpretation of surface complexation of oxalic and citric acids with hematite. *Langmuir* **1**: 195–201.

Lad, R. J., and V. E. Henrich. 1989. Photoemission study of the valence-band electronic structure in Fe_xO, Fe_3O_4, and α-Fe_2O_3 single crystals. *Phys. Rev.* **B39**: 13478–13485.

Lasaga, A. C., and A. E. Blum. 1986. Surface chemistry, etch pits and mineral-water reactions. *Geochim. Cosmochim. Acta* **50**: 2363–2379.

Lindgreen, H., J. Garnaes, P. L. Hansen, F. Besenbach, E. Laegsgaard, I. Stensgaard, S. A. Gould, and P. K. Hansma. 1991. Ultrafine particles of North Sea illite/smectite clay minerals investigated by STM and AFM. *Amer. Miner.* **76**: 1218–1222.

MacInnis, I. N., and S. L. Brantley. 1992. The role of dislocations and surface morphology in calcite dissolution. *Geochim. Cosmochim. Acta* **56**: 1113–1126.

Maurice-Johnsson, P. A. 1993. Hematite dissolution in natural organic acids: Ph.D. dissertation. Stanford University.

Miller, W. P., L. W. Zelazny, and D. C. Martens. 1986. Dissolution of synthetic crystalline and noncrystalline iron oxides by organic acids. *Geoderma* **37**: 1–13.

Ohnesorge, F., and G. Binnig. 1993. True atomic resolution by atomic force microscopy through repulsive and attractive forces. *Science* **260**: 1451–1456.

Parfitt, R. L., R. J. Atkinson, and R. St. C. Smart. 1975. The mechanism of phosphate fixation by iron oxides. *Soil Sci. Soc. of Amer. Proc.* **39**: 837–841.

Parks, G. A., and P. L. De Bruyn. 1962. The zero point of charge of oxides. *Jour. Phys. Chem.* **66**: 967–973.

Parks, G. A. 1990. Surface energy and adsorption at mineral/water interfaces: An introduction. In *Mineral-Water Interface Geochemistry*. M. F. Hochella Jr. and A. E. White, eds. Mineralogical Society of America, 133–175.

Petrovich, R. 1981. Kinetics of dissolution of mechanically comminuted rock-forming oxides and silicates—I. Deformation and dissolution of oxides and silicates in the laboratory and at the Earth's surface. *Geochim. Cosmochim. Acta* **45**: 1675–1686.

Rimstidt, J. D., and P. M. Dove. 1986. Mineral/solution reaction rates in a mixed flow reactor: Wollastonite hydrolysis. *Geochim. Cosmochim. Acta* **50**: 2509–2516.

Rude, P. D., and R. C. Aller. 1989. Early diagenetic alteration of lateritic particle coatings in Amazon continental shelf sediments. *Jour. Sed. Pet.* **59**: 704–716.

Schwertmann, U., and R. M. Cornell. 1991. *Iron Oxides in the Laboratory*. New York: VCH. 236 pp.

Schwertmann, U., W. R. Fischer, and H. Papendorf. 1968. The influence of organic compounds on the formation of iron oxides. *Trans. 9th Int. Congr. Soil Sci. Adelaide* **1**: 645–655.

Stumm, W. 1992. *Chemistry of the Solid-Water Interface*. New York: John Wiley & Sons, Inc. 428 pp.

Stumm, W., G. Furrer, E. Wieland, and B. Zinder. 1985. The effects of complex-forming ligands on the dissolution of oxides and aluminosilicates. In *The Chemistry of Weathering*. J. I. Drever, ed. Dordrecht: D. Reidel Publishing Co, 55–74.

Stumm, W., and E. Wieland. 1990. Dissolution of oxide and silicate minerals: Rates depend on surface speciation. In *Aquatic Chemical Kinetics*. W. Stumm, ed. New York: John Wiley & Sons, 367–400.

Sulzberger, B., D. Suter, C. Siffert, S. Banwart, and W. Stumm. 1989. Dissolution of Fe(III)(hydr)oxides in natural waters: Laboratory assessment on the kinetics controlled by surface coordination. *Marine Chem.* **28**: 127–144.

Sunagawa, I. 1962. Mechanism of growth of hematite. *Amer. Miner.* **47**: 1139–1155.

Sunagawa, I. 1987. Surface microtopography of crystal faces. In *Morphology of Crystals*. I. Sunagawa, ed. Tokyo: Terra Scientific Publishing Co., 321–365.

Suter, D., C. Siffert, B. Sulzberger, and W. Stumm. 1988. Catalytic dissolution of iron (III) (hydr)oxides by oxalic acid in the presence of Fe(II). *Naturwissenchaften* **75**: 571–573.

Waite, T. D., and F. M. M. Morel. 1984. Photoreductive dissolution of colloidal iron oxide: Effect of citrate. *J. Colloid Interface Sci.* **102**: 121–137.

Wehrli, B. 1989. Monte Carlo simulations of surface mor-

phologies during mineral dissolution. *J. Colloid Interface Sci.* **132**: 230–242.
Zhang, Y., N. Kallay, and E. Matijević. 1985. Interactions of metal hydrous oxides with chelating agents. 7. Hematite-oxalic acid and -citric acid systems. *Langmuir* **1**: 201–206.
Zhong, Q., D. Inniss, K. Kjoller, and V. B. Elings. 1993. Fractured polymer/silica fiber surface studied by tapping mode atomic force microscopy. *Surf. Sci. Lett.* **290**: L688–L692.

(Received 21 January 1994; accepted 30 June 1994; Ms. 2458)